Journal of Physics and Chemistry of Solids 128 (2019) 251–257

Contents lists available at ScienceDirect

Journal of Physics and Chemistry of Solids

journal homepage: www.elsevier.com/locate/jpcs

Microscopic investigation of $Bi_{2-x}Sb_xTe_{3-y}Se_y$ systems: On the origin of a robust intrinsic topological insulator

Hyoungdo Nam [a], Yang Xu [b,c], Ireneusz Miotkowski [b], Jifa Tian [b,c], Yong P. Chen [b,c,d,**], Chang Liu [e,f,1], M. Zahid Hasan [e,f], Wenguang Zhu [g], Gregory A. Fiete [a], Chih-Kang Shih [a,*]

[a] Department of Physics, The University of Texas at Austin, Austin, TX 78712, USA
[b] Department of Physics and Astronomy, Purdue University, West Lafayette, IN 47907, USA
[c] Birck Nanotechnology Center, Purdue University, West Lafayette, IN 47907, USA
[d] School of Electrical and Computer Engineering, University, West Lafayette, IN 47907, USA
[e] Joseph Henry Laboratories, Department of Physics, Princeton University, Princeton, NJ 08544, USA
[f] Princeton Institute for Science and Technology of Materials, Princeton University, Princeton, NJ 08544, USA
[g] ICQD, Hefei National Laboratory of Physical Sciences at the Microscale, Department of Physics, University of Science and Technology of China, Hefei, Anhui, 230026, PR China

ARTICLE INFO

Keywords:
Topological insulator
$BiSbTeSe_2$
Be_2Te_2Se
Aging effect
Dirac point

ABSTRACT

One of the most important challenges in the field of topological insulators (TI) is to find materials with nontrivial topological surface state (TSS) while keeping the bulk intrinsic (insulating). In this letter, we report microscopic investigations of $BiSbTeSe_2$ (1112) and Bi_2Te_2Se (221) alloys which have been proposed as candidates to achieve an intrinsic bulk. Scanning tunneling microscopy (STM) confirms previous macroscopic experiments that 221 is an ordered alloy with a Te-Bi-Se-Bi-Te sequence. Nevertheless, it also reveals that the ordering is not perfect with the surface chalcogen layer containing 85% Te and 15% Se. On the other hand, STM shows that 1112 is a random alloy with a fine mixture of (Bi, Sb) in the pnictogen layers and (Te, Se) in the top/bottom chalcogen layers. A freshly cleaved 221 sample surface shows an intrinsic bulk with the Fermi energy, E_F, in the gap, but quickly becomes n-type with aging, similar to the aging effect reported by others [27,32]. By contrast, the random alloy 1112 show remarkable robustness against aging and the E_F remains within the gap even after aging for 7 days. We attribute this result to the nanoscale fine mixture of the random alloy which provides an effective doping compensation in very fine length scale, thus enabling its bulk to remain intrinsic against aging.

1. Introduction

The ability to control the location of the Fermi level (E_F) in materials with an energy gap has played a critical role in paving the foundation of the modern semiconductor technology. For example, achieving p-type doping in GaN has resulted in transformative optoelectronic technology [1,2]. For a semiconductor, the ability to dope it n- or p-type, or to make it insulating are important [3]. In the case of three-dimensional topological insulators [4–27], the overarching goal is to achieve a robust "bulk insulating" state. This is necessary in order to realize the novel transport properties associated with the non-trivial conducting topological surface states (TSS) without the interference of bulk conduction channels. Most topological insulators are naturally n-type (such as the case of Bi_2Se_3) or p-type (such as the case of Sb_2Te_3). How to achieve a true "insulating" bulk in a TI has been one of the most important materials science challenges in this class of materials. Several strategies have been developed to achieve this goal. One approach is to synthesize the materials as pure as possible, thus eliminating potential p- or n-type doping impurities. However, this "purist's approach" is proven to be difficult: even with the most advanced fabrication (e.g., molecular beam epitaxy), where insulating Bi_2Se_3 can be initially achieved, the material can turn into n-type after aging.

Another approach is to use "dopant compensation", for example doping the usually n-type Bi_2Se_3 with p-type dopants such as Ca [24,25] and Cd [26]. Even so, it is difficult to achieve exact and homogeneous compensation. In addition, adding substantial extrinsic doping impurities

* Corresponding author. Department of Physics, The University of Texas at Austin, Austin, TX 78712, USA.
** Corresponding author. Department of Physics and Astronomy, Purdue University, West Lafayette, IN 47907, USA.
E-mail addresses: yongchen@purdue.edu (Y.P. Chen), shih@physics.utexas.edu (C.-K. Shih).
[1] Department of Physics, Southern University of Science and Technology, Shenzhen 518055, China.

https://doi.org/10.1016/j.jpcs.2017.10.026
Received 1 March 2017; Received in revised form 17 August 2017; Accepted 20 October 2017
Available online 23 October 2017
0022-3697/Published by Elsevier Ltd.

often increases the disorder and degrade the transport properties of the system. A third approach is to form an alloy by mixing Bi_2Se_3, Bi_2Te_3, and Sb_2Te_3 with some compositional ratios to $Bi_{2-x}Sb_xTe_{3-y}Se_y$ [28–36]. This alloying approach appears to have yield fruitful results. Angle-resolved photoemission spectroscopy (ARPES) investigations suggest the existence of an optimal alloy composition where E_F is stabilized near the Dirac point (DP) in the bulk band gap [33]. Recent observation of a TSS quantum Hall effect in $Bi_1Sb_1Te_1Se_2$, further marks an important milestone in demonstrating surface-dominated conduction [36]. The key question is "Why some alloys exhibit a robust insulating bulk while some do not?" Understanding its microscopic origin holds the key for the rational design of better TI materials for realization of their novel properties originating in the non-trivial topological surface states.

In this letter, we address these critical questions by using scanning tunneling microscopy and spectroscopy (STM/S) to investigate $Bi_{2-x}Sb_xTe_{3-y}Se_y$ alloys with two stoichiometric compositions– the Bi_2Te_2Se ($x = 0$, $y = 1$; referred to as 221) and $BiSbTeSe_2$ ($x = 1$, $y = 2$; referred to as 1112). Although both compositions allow the *possibility* of ordering arrangement of constituents in the quintuple layer (QL), we confirm that only the 221 compound exhibits this tendency with a Te-Bi-Se-Bi-Te sequence [28,37]. On the other hand, the 1112 sample is a *random* alloy [38]. This conclusion is corroborated with X-ray diffraction (XRD) patterns. First principle calculations of energetics indeed show that the 221 favors order alloy formation with Te-Bi-Se-Bi-Te and the 1112 has a tendency to form random alloys. STS measurements show that the ordered 221 alloy surface will eventually turn into n-type after aging in ultrahigh vacuum (UHV) of 4×10^{-11} Torr. Most interestingly, the 1112 random alloy shows a robust insulating bulk with E_F pinned near the DP in spite of the random compositional fluctuation, line defects, and time spent in the same condition as the 221, aside from the longer span of 7 days. In fact, it appears that the random mixture in a fine length scale could be a cause of the pinned E_F in this material.

2. Structural characterizations and modeling

2.1. Bi_2Te_2Se

Fig. 1a, d are topographic images at an atomic scale, taken on the top layers of 221 and 1112, respectively. In the case of 221, the image has an apparent binary contrast: the atomic sites are either bright or dark. Note that the dark site is not a vacancy because the local corrugation peak can be observed (see line profile of Fig. 1b and appearance of a vacancy from the building block model of Fig. 1g). The height difference between the bright and dark sites is ~60 p.m., which is significantly smaller than the interlayer distance on the order of 200 p.m. in a QL. Moreover, the bight/dark contrast remains the same even when the bias polarity is reversed (see Supporting Information Figs. S1a and b). This binary feature most likely comes from different kinds of chalcogens, such as Se and Te, on the homogenous underlying pnictogen (Bi) layer. By using the atomic radii (1.19 Å for Se, 1.42 Å for Te, and 1.50 Å for Bi), we construct a model of Fig. 1h and i for dilute Se on the surface layer and obtain a height difference of 52 p.m. between Te and Se, consistent with the experimental observation of 60 p.m. (Note that if local density of states variation strongly contributes to the STM image of 221, it is expected not to localize at one atomic scale but to extend by several lattice sites; for example, defects in Bi_2Se_3 [8].) Counting the number of bright and dark atoms on Fig. 1a, the occupation ratio of Te to Se is 6:1, which is larger than the compositional ratio of 2:1. In addition, the XRD pattern taken on the same batch of 221 (Fig. 1c) shows the characteristic peaks at (1,0,7), and (0,0,12), which imply that Se mainly occupies the center layer in a QL of 221 [28,37,38]. All results of STM, the building block model, and XRD reflect that 221 is based on an ordered arrangement with the QL dominantly comprising the Te-Bi-Se-Bi-Te sequence of atomic layers. Nevertheless, the degree of ordering is not perfect as STM shows that only 85% of surface sites are occupied by Te instead of 100% for a perfectly ordered alloy.

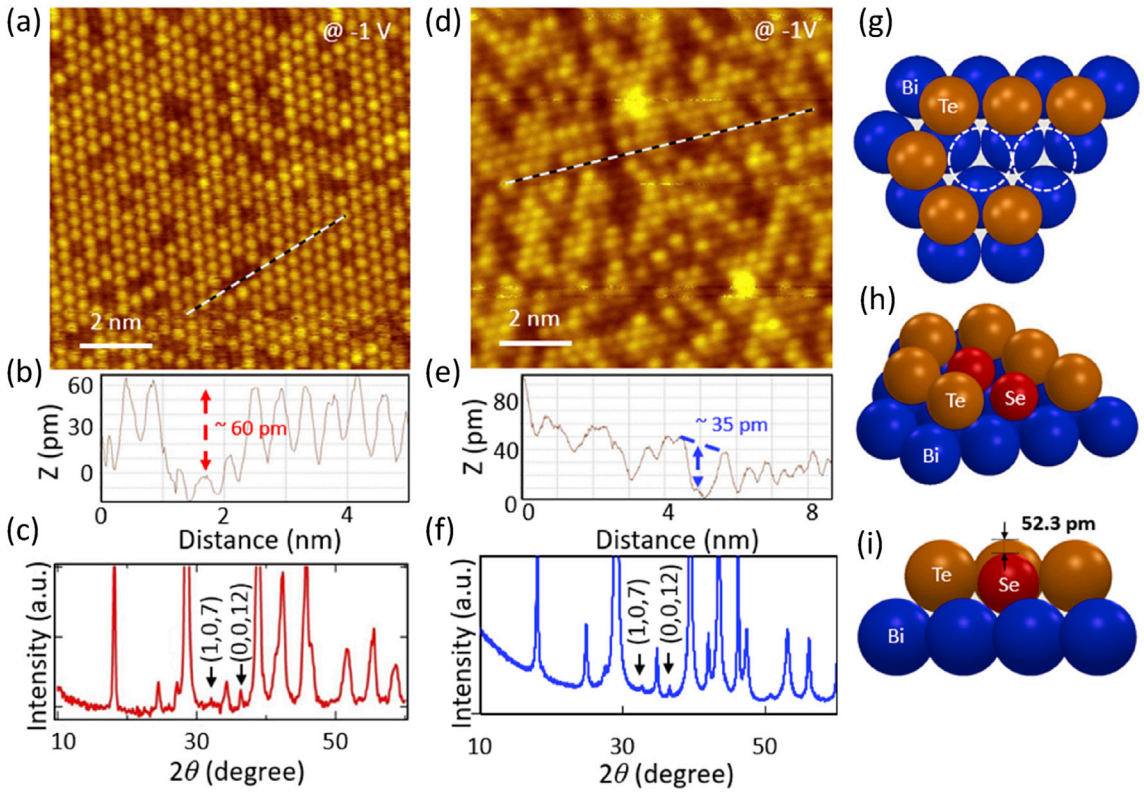

Fig. 1. (a and d) Atomic resolution topographic images on the surfaces of (a) 221 and (d) 1112. (b and e) Line profiles along the white dashed lines in (a) and (d), revealing the height differences of 60 p.m. and 35 p.m. for each sample. (c and f) X-ray powder diffraction pattern on the pieces of the same batches of (c) 221 and (f) 1112. (g and h) Building block models of the most top two layers in a QL for the case of (g) Te-vacancies and (h) Se-substitutions. (i) Lateral view of (h), revealing the height difference of 52.3 p.m.

2.2. $BiSbTeSe_2$

In contrast to 221, the topographic image on 1112 (Fig. 1d) has a complicated color contrast. Although the line profile of Fig. 1e shows the atoms of diverse heights on different background modulation slopes, the largest height difference of ~35 p.m. among the nearest neighbor atoms is even shorter than in the case of 221. This result rules out the possibility of a homogeneous pnictogen layer (Bi or Sb). Moreover, the polarity dependent images do not have the same contrast: some fraction of bright atoms become dark and some dark ones become bright when the sample bias polarity changes (see Supporting Information Figs. S1c,d and S2). Although quantitative determinations of individual Te/Se locations are difficult due to this complexity, one can still draw a qualitative conclusion. Note the intermingling of dark and bright features at the nanometer scale. Structurally, the height not only reflects the chemical species of the top layer (Te versus Se), but also is influenced by the local chemical species in the pnictogen layer below. The local combination probably also influences the polarity dependent image. The lack of the regularity in the voltage dependent topographic heights and the apparent intermixing of dark and bright features at the nanometer scale suggest a random mixture in the top chalcogen layer (Te and Se) and the next pnictogen layer (Bi and Sb). Based on the structural symmetry, one can infer that the bottom chalcogen and pnictogen layers should also contain a random mixture. However, the center chalcogen layer remains unknown. The XRD on the same batch of 1112 (Fig. 1f) shows the same characteristic peaks at (1,0,7) and (0,0,12) as 221, suggesting the center layer is mainly occupied by Se atoms [38]. One can therefore conclude that 1112 has a random arrangement in a QL, such as Te/Se-Bi/Sb-Se-Bi/Sb-Te/Se with a total Bi:Sb:Te:Se ratio of 1:1:1:2.

2.3. Theoretical analysis

To understand the observed difference in the formation of 221 and 1112 alloys, we performed first-principles density functional theory (DFT) calculations to compare the total energies of freestanding single QLs in different chemical compositions. For the 221 case, there are only two possible sequences, Te-Bi-Se-Bi-Te and Te-Bi-Te-Bi-Se. The calculation results show that the Te-Bi-Se-Bi-Te is lower in energy than the Te-Bi-Te-Bi-Se by 0.16 eV. For the 1112 case, there are three possible sequences, Se-Bi-Se-Sb-Te, Te-Bi-Se-Sb-Se, and Se-Bi-Te-Sb-Se, among which the Se-Bi-Se-Sb-Te is energetically most stable. The Te-Bi-Se-Sb-Se has a slightly higher energy of 0.09 eV and the Se-Bi-Te-Sb-Se a higher energy of 0.20 eV than the most stable Se-Bi-Se-Sb-Te arrangement. All these results indicate that both alloys show the same tendency that Te strongly favors the outer chalcogen layer and the central chalcogen layer is preferred by Se. For the 1112 alloys, the small energy difference (0.09 eV) between Te-Bi-Se-Sb-Se and Se-Bi-Se-Sb-Te might be too small to lead to any significant difference in the probability of their occurrence in actual samples, which corroborate the evidences of STM and XRD that the 1112 tends to form the mixture of the two low energy phases – namely random mixtures in the two outer chalcogen and pnictogen layers but leaving the center chalcogen layer predominantly occupied by Se. In contrast, the much larger energy difference (0.16 eV) between the two stacking sequences in the 221 alloys may result in a strong tendency to form ordered alloys (the Te-Bi-Se-Bi-Te sequence), consistent with the experimental observation.

3. Electronic characterization

3.1. d^2I/dV^2 tunneling spectroscopy

We next discuss the result of spectroscopic investigations. As a reference, Fig. 2a shows a typical dI/dV tunneling spectrum (red solid) acquired on the freshly cleaved surface of Bi_2Se_3, a system that had been thoroughly investigated previously using ARPES and STS. In this spectrum, the DP can be clearly located at −0.3 eV below the E_F. Above and below the DP dI/dV exhibits a linear dependence, consistent with the linear (in energy) density of states (DOS). The locations of the valence band maximum (VBM) and the conduction band minimum (CBM) have been shown before to be located at ~ 0.1 eV below and 0.2 eV above the DP, respectively. They roughly correspond to the location where slope in dI/dV spectrum starts to change. The second derivative, d^2I/dV^2, enhances the features of the VBM and CBM thresholds more clearly. It is important to bear in-mind that the d^2I/dV^2 is used here only to enhance the spectral features and is not related to inelastic tunneling.

3.2. Aging effect on Bi_2Te_2Se

On the 221 surfaces, we carried out spectroscopic investigations to study the aging effect, as shown in Fig. 2b. The freshly cleaved surface was transferred to the LT-STM in less than 3 min to perform the dI/dV (STS) measurements. Then, the aging is performed by taking the sample out of the LT-STM stage but leaving it in the UHV chamber on a sample stage kept at room temperature. After the desired aging time is reached, the sample is then moved back to LT-STM stage for STS investigation. On the surface of 221 samples, the DP is below the VBM, as shown by the ARPES data in Fig. 2c measured on another sample from the same batch. Thus, the dip position in the dI/dV spectrum does not correspond to the DP. For the freshly cleaved surface, there is an apparent gap with E_F in the gap. Upon aging, however, the surface quickly turns into n-type, reflected by the leftward shift of the spectral features. Within the gap, there is a region with linear slope in the dI/dV spectrum, corresponding to the TSS whose DOS has a linear energy dependence. The assignment of the energy locations of the VBM and CBM, however, is somewhat non-trivial and some assumptions need to be made. We use the spectrum with 30 min aging (middle panel) for discussion since individual thresholds are more well-defined. The TSS, appearing as a linear energy dependence in dI/dV would appear as a constant in the d^2I/dV^2 spectrum. The transition to the conduction band can be identified as the change in the d^2I/dV^2 and the CBM is labeled at the mid-point of this transition, which is about 30 meV above E_F. If we use the same criterion to assign the location of the VBM, it would occur at about 220 meV below E_F. These assignments will yield a bandgap of 0.25 eV, which is 0.05 eV smaller than that determined using ARPES. Taking a gap value of 0.30 eV, the VBM should be located at −0.27 eV (marked by a black arrow). Since our goal is to investigate the *relative* movement of band structure upon aging, this uncertainty in the precise determination of the VBM location does not influence our scientific conclusion.

After 3 days of aging, the surface becomes even more n-type and the dip in the dI/dV spectrum is shifted further downward by about 0.07 eV. This should place the CBM location at 40 meV below E_F. Interestingly, the spectroscopic features near the CBM start to show some structure: instead of a simple increase, the slope in dI/dV first decreases then increases again as the bias voltage is moved into the conduction band. This might be due to the formation of 2D electron gas resulting from a strong surface band bending [39,40], which now also contributes to the tunneling spectrum. We have seen this consistently when the surface becomes deeply n-type. This observation, while being interesting and warranting further investigations, is beyond the scope of this paper. Thus, although the freshly cleaved 221 sample surface indeed exhibits intrinsic semiconducting properties, upon aging it quickly becomes n-type and eventually becomes degenerate n-type similar to that of Bi_2Se_3. We note that previously aging effect has been investigated using STS [27] and ARPES [32] by intentionally introducing adsorbates/molecules on samples.

3.3. Band structure of $BiSbTeSe_2$

On the other hand, the 1112 sample exhibits a totally different behavior. The left of Fig. 3a is a typical dI/dV spectrum (red solid) acquired on 1112 surfaces. Although this dI/dV shows much smoother features rather than the others, we are able to label the DP, VBM, and CBM with the help of the d^2I/dV^2 spectrum. Shown on the right are the

simulation results for dI/dV and d^2I/dV^2 spectra by using the designated locations of the CBM, DP, and VBM, which well reproduce the observed features (details described in Supporting Information Fig. S3). Note that the DP is located at the position where $d^2I/dV^2 = 0$, because the TSS contribution to dI/dV has a V-shape around the DP and the d^2I/dV^2 curve is suddenly turned over from negative to positive there. In this particular spectrum, the DP is located nearly at E_F while the VBM is at ~90 meV below DP and CBM at ~220 meV above the DP. ARPES data of Fig. 3b corroborates the analysis of the d^2I/dV^2 spectrum. DP appears at E_F (the left of Fig. 3b) and the constant energy map at $E_B = -90$ meV (the right of Fig. 3b) reveals points of VBM in addition to a small circle of TSS at the center. This result is also consistent with previous ARPES studies [33].

3.4. Fermi level pinning in the band gap of $BiSbTeSe_2$

The structural investigations above show that 1112 contains a random mixture of constituents. This implies that there must exist compositional fluctuations. One can ask about the local fluctuations of the DP in the presence of such a compositional fluctuation. Fig. 3c and d are the STM images where the current image tunneling spectroscopy (CITS) is acquired (32 × 32 pixels) and the corresponding spatial variation of the DP deduced from the scanning tunneling spectra. There does not appear to be a spatial correlation between the DP distribution and the STM image. We note that a direct determination of the actual composition cannot be obtained at the present time due to the complicated bias dependent image (see Supporting Information Figs. S1c,d and S2) as the mixtures in the chalcogen layer and the pnitcogen layer can both impact the STM image. Nevertheless, one can still conclude that the change in topographic contrast is due to the composition change. One important issue to be addressed is the statistical distribution of the DP relative to E_F in this random alloy. Shown in Fig. 3e is the distribution of the DP deduced from 1024 spectra acquired in a local region of 5 nm by 5 nm. Statistically, it shows an average DP position at 8 meV above E_F with a full width at half maximum (FWHM) of 34 meV. Investigations are carried out over several different regions (several microns apart) and the results are very similar: The DP is located near E_F with a distribution between 20 and 30 meV.

The above spectroscopic investigations show that despite large compositional fluctuations in 1112, E_F is stably pinned near the Dirac point within the bulk band gap. Moreover, this stability is maintained against the aging effect, in contrast to 221. As shown in Fig. 4d, E_F is stably pinned near the DP of −25 meV even after aging for 7 days. But perhaps the most notable result is that this stability is maintained even near a line defect, such as the one shown in Fig. 4a. Such line defects are occasionally observed on the cleaved 1112 surface, whose width is ~10 nm and height is ~90 p.m. On the defect line, while an additional shoulder feature in the dI/dV is observed above (but near) E_F, the DP is still pinned down near E_F. Those observations directly show the robustness of E_F and TSS in the 1112, regardless of aging and defect lines as well as random alloy fluctuation. But what causes this robust E_F pining in the band gap?

We first note that the fine mixture of parent compounds at nanometer scales appears to play a critical role. The fine grain mixture first ensures a compositional average of the electronic structures with DP in the gap. Second, bulk Sb_2Te_3 and Bi_2Te_3 often have tendencies to be p-type while Bi_2Se_3 tends to be n-type. Regardless exactly what kind of defects are responsible for their p- and n-type behavior, we speculate that a fine grain mixture may *force* the chemical potential to lie within the gap and responsible for a robust E_F pinning. This case may be similar to the pursuit of creating semi-insulating GaAs where the breakthrough came

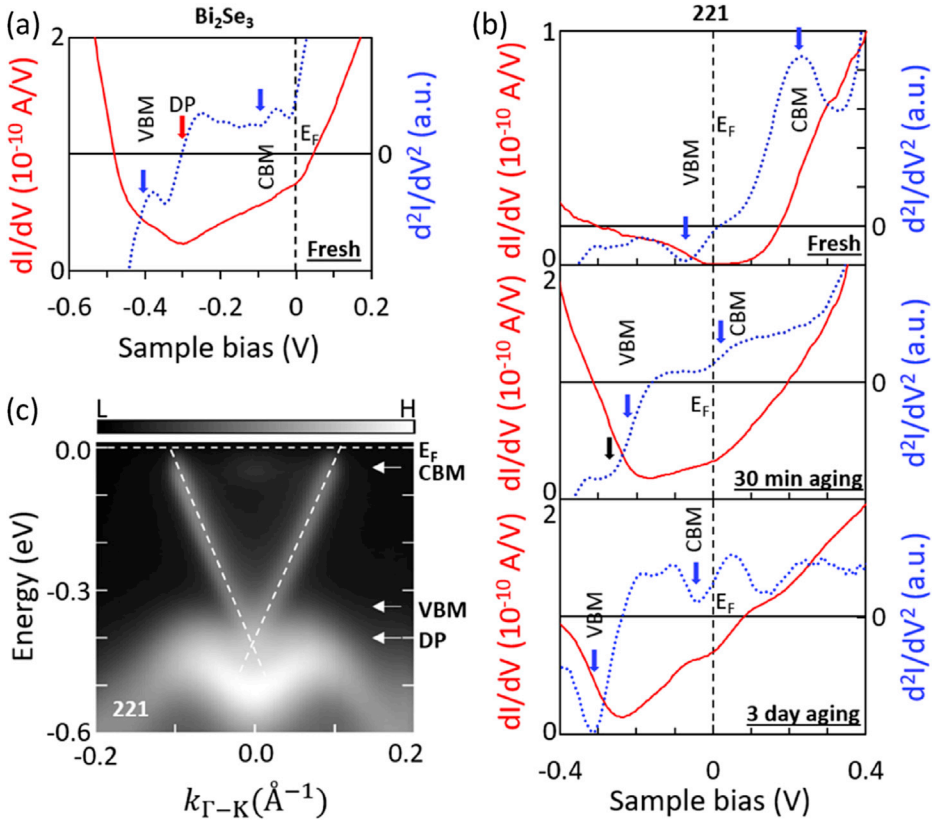

Fig. 2. (a) dI/dV (red solid) and d^2I/dV^2 (blue dot) tunneling spectra on the fresh cleaved surface of n-type Bi_2Se_3. (b) Tunneling spectra on the fresh cleaved surface of 221, showing the intrinsic TI feature (top). Since DP of 221 is buried in valence band, there is no V-shape linear dispersion feature in dI/dV curve unlike Bi_2Se_3. After UHV-R annealing for 30 min, E_F is just below CB, which implies the sudden change of E_F about 0.2 eV (middle). After UHV-RT annealing for 3 days, 221 became n-type (bottom). Note that the conduction band kept changing with annealing. (c) Band dispersion of 221 along —K-Γ-K, measured by ARPES and matched with tunneling spectra of 3 day-aged 221. (For interpretation of the references to colour in this figure legend, the reader is referred to the web version of this article.)

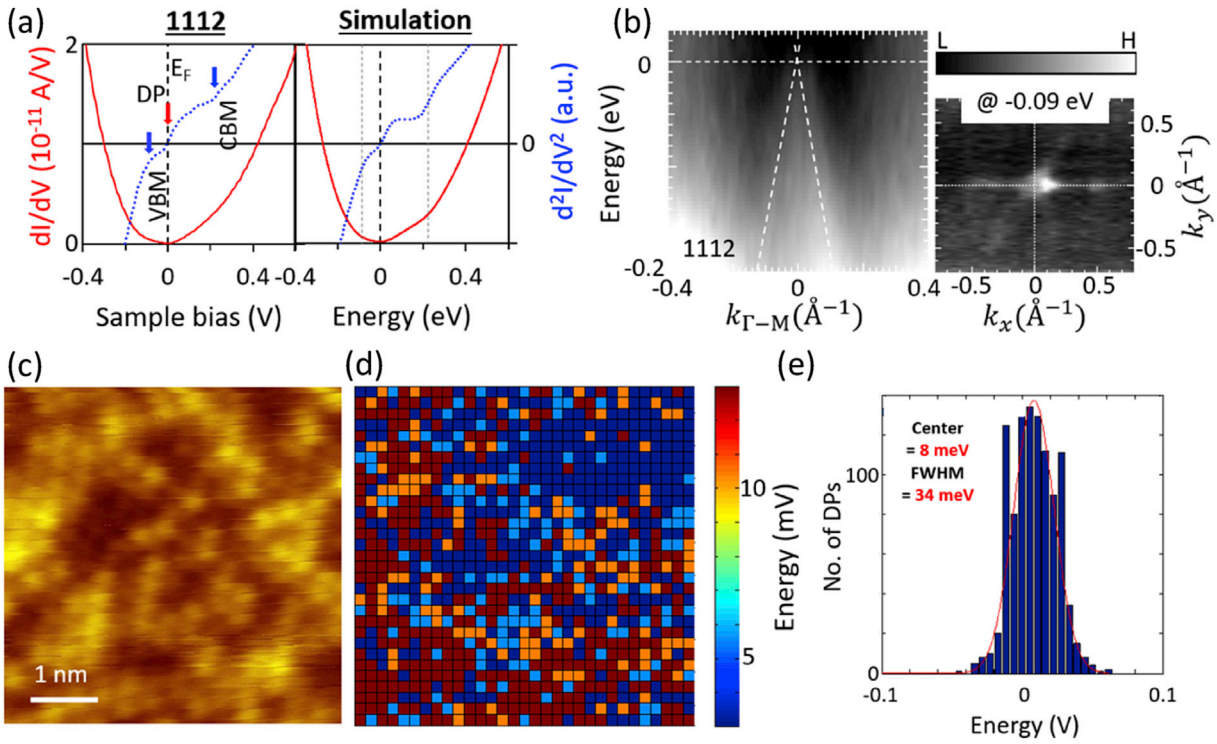

Fig. 3. (a) Experimental data and its simulation result of dI/dV (red solid) and d^2I/dV^2 (blue dot) tunneling spectra on 1112 at 77 K. (b) Band dispersion along –M-Γ-M and constant energy map at E = −0.09 eV, measured by APRES. (c) Topographic images of CITS. (d) DPs' distribution from CITS using d^2I/dV^2 spectroscopy. (e) The statistic profile of DPs of (d). Gaussian fit gives that FWHM is 34 meV, centered at 8 meV. (For interpretation of the references to colour in this figure legend, the reader is referred to the web version of this article.)

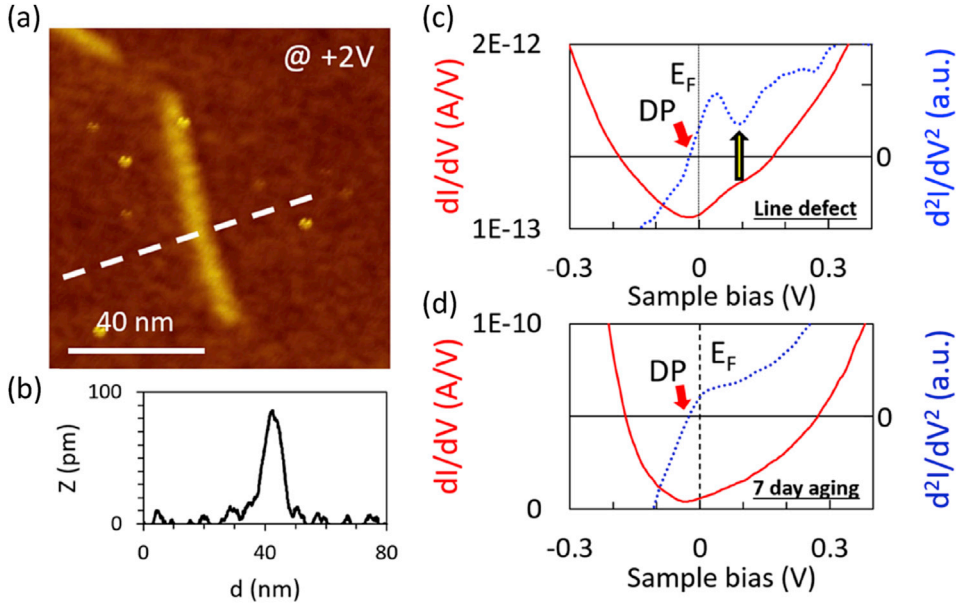

Fig. 4. (a) Topographic image of a line defect on 1112. (b) The line profile along the white dashed line in (a). The height and width of the line defect are 0.9 Å and 10 nm, respectively. (c) dI/dV and d^2I/dV^2 tunneling spectra obtained at the center of line defect. The defect state and DP are marked with yellow and red arrows, respectively. (d) dI/dV and d^2I/dV^2 tunneling spectra after aging 1112 in UHV at RT for 7 days. (For interpretation of the references to colour in this figure legend, the reader is referred to the web version of this article.)

from the incorporation of As anti-site defects to pin the E_F in the mid gap [3].

4. Conclusions

In summary, we have studied the atomic structure and the local electronic structure of $Bi_{2-x}Sb_xTe_{3-y}Se_y$ using STM/S. Analysis of atomic STM images confirms the previous macroscopic reports [28,37,38] that the 221 material is an ordered alloy with Te-Bi-Se-Bi-Te sequence although 221 surface sites are occupied by only 85% Te atoms instead of 100%. On the other hand, the 1112 material is a random alloy with Te/Se-Bi/Sb-Se-Bi/Sb-Te/Se sequence (except that the center layer of the quintuple layer is likely to be occupied mainly by Se), consistent with X-ray diffraction and DFT calculation. Compared with dI/dV spectroscopy, d^2I/dV^2 enhances the spectroscopic features to allow us to identify the Dirac point, the conduction band minimum, and the valence band

maximum more unambiguously, which are confirmed by ARPES. In contrast to the ordered alloy 221, the most intriguing observation is the remarkable affinity between the Dirac point and E_F in the 1112 material with respect to random composition fluctuations, line defects, and the aging effect. We suggest that the fine mixture of parent compounds at small length scale may play a very beneficial role in balancing the chemical potential, resulting in a stable Fermi level pinning in the band gap and giving rise to the robust insulating states. It further suggests that random alloys consisting of a mixture of inherent p-doped TI and n-doped TI at a fine length scale (nm) offers a promising material design route for optimized topological insulator properties. We notice that a similar conjecture was used in a recent theoretical study by Skinner et al. [45]. Nevertheless, the observed resistivity of 1112 compound in the current study [36] is higher than the predicted upper limit of Ref. [45].

4.1. Methods

The single crystals of 221 and 1112 were grown by the Bridgman method using two-step procedures. In the first step, the raw material was synthesized in a two-zone horizontal furnace with independent temperature control. The starting materials of 6 N purity were first deoxidized before use. Additionally, to minimize the concentration of uncontrolled impurities both Te and Se were purified further by multiple vacuum distillations under dynamic vacuum of 10^{-7} Torr.

The synthesis from the starting materials taken appropriate stoichiometric proportions was performed in vitreous carbon boats placed into carbonized ampoules to avoid contamination from quartz. The ampoules sealed under vacuum of 10^{-7} Torr were allowed for a preliminary reaction of the components at 400 °C and subsequently heated up (for approximately 6 h) to 740 °C (for 221) and 680 °C (for 1112), respectively. The temperature of the pre-reacted charge was then increased to 850–900 °C and held for 24 h to allow melt homogenization under a controlled pressure of Se. After homogenization, the ampoules were cooled down slowly to about 600 °C (for 221) and 550 °C (for 1112), respectively, to let homogenization of the solidified charge.

In the next step, the charge was transferred into a carbonized quartz ampoule and placed into a two-zone vertical high-temperature Bridgman furnace. The temperature profile was regulated by changing a distance between heating zones. The ampoules were heated up to 850 °C and then hold for several hours to let homogenization of the melt. The axial linear gradient in the growth zone was set to 12 ºC/cm for 221 and 25 ºC/cm 1112, respectively. The radial gradient inside the growth zone was symmetric and estimated to be less than 0.5 ºC/cm. The single crystals were grown with a rate of approximately 1–1.5 mm/h. The solidified crystals were homogenized at 580–600 °C (for 221) and/or 540–560 °C (for 1112) for 6 h and then cooled down to room temperature.

For STM measurement, samples were cleaved in an UHV chamber of 4×10^{-11} Torr at RT and quickly transferred (within 3 min) into the low temperature scanning tunneling microscope (LT-STM) stage operating at 77 K. The aging effect is investigated by transferring the sample into a station held at RT in the same chamber, then transferring back into the LT-STM stage for investigation. STS is the averaged spectrum of 64 or 256 point spectra on 5 nm × 5 nm area. ARPES measurement for 1112 was performed at Beamline 10.0.1 (HERS) of the Advanced Light Source, Berkeley, California, using a VG-Scienta R4000 electron analyzer; for 221, ARPES was carried out at the APPLE-PGM beam line of the Synchrotron Radiation Center (SRC), Wisconsin, using a VG-Scienta 200U electron analyzer. Energy resolution was set to be ~20 meV.

The DFT calculations were carried out using the projector augmented wave method [41,42] with the generalized gradient approximation in the parametrization of Perdew, Burke and Enzerhof [43] for the exchange correlations as implemented in the Vienna Ab Initio Simulation Package [44]. A plane-wave energy cutoff of 250.0 eV was consistently used in all the calculations. The supercells contain a unit cell of the QL structure with a vacuum region of more than 15 Å. A 9 × 9 × 1 special **k**-point mesh including the Γ point (0,0,0) was used for integration over the Brillouin zone. The in-plane crystal parameters of freestanding single QLs were fully optimized. Optimized atomic structures were achieved when forces on all the atoms were less than 0.01 eV/Å.

5. Notes

The authors declare no competing financial interest.

Acknowledgment

STM/S measurements performed at UT-Austin were supported by the NSF DMR-1506678 and the Welch Foundation (F-1672). 3D TI growth and XRD measurements were carried at PU via the support of DARPA MESO program (Grant N66001-11-1-4107). The angle resolved photoemission measurements were also support by the DARPA MESO program (Grant N66001-11-1-4107). DFT calculations at USTC were supported by the National Natural Science Foundation of China (Grant No. 11374273) and the Fundamental Research Funds for the Central Universities (Grant Nos. WK2090050027, WK2060190027, WK2340000063) and performed at National Supercomputing Center in Tianjin. Theoretical work at UT was supported by NSF DMR-1507621 and ARO W911NF-14-1-0579.

Appendix A. Supplementary data

Supplementary data related to this article can be found at https://doi.org/10.1016/j.jpcs.2017.10.026.

References

[1] S. Nakamura, T. Muaki, M. Senoh, N. Iwasa, Jpn. J. Appl. Phys. 31 (1992) L139.
[2] H. Amano, M. Kito, K. Hiramatsu, I. Akasaki, Jpn. J. Appl. Phys. 28 (1989) L2112.
[3] A.C. Warren, J.M. Woodall, J.L. Freeouf, D. Grischkowsky, D.T. McInturff, M.R. Melloch, N. Otsuka, Appl. Phys. Lett. 57 (1990) 1331.
[4] D. Hsieh, D. Qian, L. Wray, Y. Xia, Y.S. Hor, R.J. Cava, M.Z. Hasan, Nature 452 (2008) 970.
[5] J.E. Moore, Nature 464 (2010) 194.
[6] P.D.C. King, R.C. Hatch, M. Bianchi, R. Ovsyannikov, C. Lupulescu, G. Landolt, B. Slomski, J.H. Dil, D. Guan, J.L. Mi, E.D.L. Rienks, J. Fink, A. Lindblad, S. Svensson, S. Bao, G. Balakrishnan, B.B. Iversen, J. Osterwalder, W. Eberhardt, F. Baumberger, Ph. Hofmann, Phys. Rev. Lett. 107 (2011) 096802.
[7] Y. Zhang, K. He, C.Z. Chang, C.L. Song, L.L. Wang, X. Chen, J.F. Jia, Z. Fang, X. Dai, W.Y. Shan, S.Q. Shen, Q. Niu, X.L. Qi, S.C. Zhang, X.C. Ma, Q.K. Xue, Nat. Phys. 6 (2010) 584.
[8] C. Mann, D. West, I. Miotkowski, Y.P. Chen, S. Zhang, C.K. Shih, Nat. Comm. 4 (2013) 2277.
[9] Y. Ando, T. Hamasaki, T. Kurokawa, K. Ichiba, F. Yang, M. Novak, S. Sasaki, K. Segawa, Y. Ando, M. Shiraishi, Nano Lett. 14 (2014) 6226.
[10] C.L. Kane, E.J. Mele, Phys. Rev. Lett. 95 (2005) 146802.
[11] Y.S. Fu, M. Kawamura, K. Igarashi, H. Takagi, T. Hanaguri, T. Sasagawa, Nat. Phys. 10 (2014) 815.
[12] B. Xia, P. Ren, A. Sulaev, P. Liu, S.Q. Shen, L. Wang, Phys. Rev. B 87 (2013), 085442.
[13] H. Zhang, C.X. Liu, X.L. Qi, X. Dai, Z. Fang, S.C. Zhang, Nat. Phys. 5 (2009) 438.
[14] Y. Xia, D. Qian, D. Hsieh, L. Wray, A. Pal, H. Lin, A. Bansil, D. Grauer, Y.S. Hor, R.J. Cava, M.Z. Hasan, Nat. Phys. 5 (2009) 398.
[15] S. Urazhdin, D. Bilc, S.D. Mahanti, S.H. Tessmer, T. Kyratsi, M.G. Kanatzidis, Phys. Rev. B 69 (2004), 085313.
[16] M. Bianchi, R.C. Hatch, J. Mi, B.B. Iversen, P. Hofmann, Phys. Rev. Lett. 107 (2011) 086802.
[17] H.M. Benia, C. Lin, K. Kern, C.R. Ast, Phys. Rev. Lett. 107 (2011) 177602.
[18] D. Hsieh, Y. Xia, D. Qian, L. Wray, F. Meier, J.H. Dil, J. Osterwalder, L. Patthey, A.V. Fedorov, H. Lin, A. Bansil, D. Grauer, Y.S. Hor, R.J. Cava, M.Z. Hasan, Phys. Rev. Lett. 103 (2009), 146401.
[19] H.J. Noh, H. Koh, S.J. Oh, J.H. Park, H.D. Kim, J.D. Rameau, T. Valla, T.E. Kidd, P.D. Johnson, Y. Hu, Q. Li, Europhys. Lett. 81 (2008), 57006.
[20] Y.L. Chen, J.G. Analytis, J.H. Chu, Z.K. Liu, S.K. Mo, X.L. Qi, H.J. Zhang, D.H. Lu, X. Dai, Z. Fang, S.C. Zhang, I.R. Fisher, Z. Hussain, Z.X. Shen, Science 325 (2009) 178.
[21] Y. Jiang, Y. Wang, M. Chen, Z. Li, C. Song, K. He, L. Wang, X. Chen, X. Ma, Q.K. Xue, Phys. Rev. Lett. 108 (2012), 016401.
[22] D. Kong, W. Dang, J.J. Cha, H. Li, S. Meister, H. Peng, Z. Liu, Y. Cui, Nano Lett. 10 (2010) 2245.

[23] J.G. Analytis, R.D. McDonald, S.C. Riggs, J.H. Chu, G.S. Boebinger, I.R. Fisher, Nat. Phys. 6 (2010) 960.
[24] Y.S. Hor, A. Richardella, Y. Xia, J.G. Checkelsky, A. Yazdani, M.Z. Hasan, N.P. Ong, R.J. Cava, Phys. Rev. B 79 (2009), 195208.
[25] J.G. Checkelsky, Y.S. Hor, R.J. Cava, N.P. Ong, Phys. Rev. Lett. 106 (2011), 196801.
[26] Z. Ren, A.A. Taskin, S. Sasaki, K. Segawa, Y. Ando, Phys. Rev. B 84 (2011), 075316.
[27] C. Durand, X.-G. Zhang, S.M. Hus, C. Ma, M.A. McGuire, Y. Xu, H. Cao, I. Miotkowski, Y.P. Chen, A.-P. Li, Nano Lett. 16 (2016) 2213.
[28] Z. Ren, A.A. Taskin, S. Sasaki, K. Segawa, Y. Ando, Phys. Rev. B 82 (2010), 241306R.
[29] S. Jia, H. Ji, E. Climent-Pascual, M.K. Fuccillo, M.E. Charles, J. Xiong, N.P. Ong, Phys. Rev. B 84 (2011), 235206.
[30] J. Xiong, A.C. Petersen, D. Qu, Y.S. Hor, R.J. Cava, N.P. Ong, Phys. E 44 (2012) 917.
[31] J. Zhang, C.Z. Chang, Z. Zhang, J. Wen, X. Feng, K. Li, M. Liu, K. He, L. Wang, X. Chen, Q.K. Xue, X. Ma, Y. Wang, Nat. Comm. 2 (2011) 574.
[32] A.A. Taskin, Z. Ren, S. Sasaki, K. Segawa, Y. Ando, Phys. Rev. Lett. 107 (2011) 016801.
[33] T. Arakane, T. Sato, S. Souma, K. Kosaka, K. Nakayama, M. Komatsu, T. Takahashi, Z. Ren, K. Segawa, Y. Ando, Nat. Comm. 3 (2012) 636.
[34] S. Kim, S. Yoshizawa, Y. Ishida, K. Eto, K. Segawa, Y. Ando, S. Shin, F. Komori, Phys. Rev. Lett. 112 (2014) 136802.
[35] W. Ko, I. Jeon, H.W. Kim, H. Kwon, S.J. Kahng, J. Park, J.S. Kim, S.W. Hwang, H. Suh, Sci. Rep. 3 (2014) 2656.
[36] Y. Xu, I. Miotkowski, C. Liu, J. Tian, H. Nam, N. Alidoust, J. Hu, C.K. Shih, M.Z. Hasan, Y.P. Chen, Nat. Phys. 10 (2014) 956.
[37] O.B. Sokolov, S.Y. Skipidarov, N.I. Duvankov, G.G. Shabunina, J. Cryst. Growth 262 (2004) 442.
[38] Z. Ren, A.A. Taskin, S. Sasaki, K. Segawa, Y. Ando, Phys. Rev. B 84 (2011), 165311.
[39] M. Bianchi, D. Guan, S. Bao, J. Mi, B.B. Iversen, P.D.C. King, P. Hofmann, Nat. Comm. 1 (2010) 128.
[40] C. Chen, S. He, H. Weng, W. Zhang, L. Zhao, H. Liu, X. Jia, D. Mou, S. Liu, J. He, Y. Peng, Y. Feng, Z. Xie, G. Liu, X. Dong, J. Zhang, X. Wang, Q. Peng, Z. Wang, S. Zhang, F. Yang, C. Chen, Z. Xu, X. Dai, Z. Fang, X.J. Zhou, PNAS 109 (2012) 3694.
[41] P.E. Blöchl, Phys. Rev. B 50 (1994) 17953.
[42] G. Kresse, D. Joubert, Phys. Rev. B 59 (1999) 1758.
[43] J.P. Perdew, K. Burke, M. Ernzerhof, Phys. Rev. Lett. 77 (1996) 3865.
[44] G. Kresse, J. Furthmüller, Phys. Rev. B 54 (1996) 11169.
[45] B. Skinner, T. Chen, B.I. Shklovskii, Phys. Rev. Lett. 109 (2012), 176801.